inorganics

MDPI

Article

A Reliable Method for the Preparation of Multiporous Alumina Monoliths by Ice-Templating

Jérémy Dhainaut [1,2], Sylvain Deville [1], Idris Amirouche [1,3] and Michaela Klotz [1,*]

[1] Laboratoire de Synthèse et Fonctionnalisation des Céramiques, UMR3080, CNRS/Saint-Gobain, 550 Avenue Alphonse Jauffret, F-84306 Cavaillon Cedex, France; jeremy.dhainaut@ircelyon.univ-lyon1.fr (J.D.); Sylvain.deville@saint-gobain.com (S.D.); Idris.Amirouche@saint-gobain.com (I.A.)

[2] Present address: Institut de Recherches sur la Catalyse et l'Environnement de Lyon – IRCELYON, UMR5256 CNRS-Université Claude Bernard Lyon 1, 2 Avenue Albert Einstein, F-69626 Villeurbanne Cedex, France

[3] Present address: Saint-Gobain Lumilog, F-06220 Vallauris, France

* Correspondence: Michaela.klotz@saint-gobain.com; Tel.: +33-4-3250-0921; Fax: +33-4-3250-0971

Academic Editors: Samuel Bernard, André Ayral and Philippe Miele

Received: 15 January 2016; Accepted: 1 March 2016; Published: 11 March 2016

Abstract: Alumina supports presenting a bimodal porosity are generally advantageous for the conversion of bulky molecules such as found in biomass, refining, and petrochemistry. However, shaping of such materials, while controlling pores size and orientation, proves to be hard. This problem can be tackled by using a simple method involving sol-gel chemistry, surfactant self-assembly, and ice-templating. Herein, a systematic study of the formulation and process parameters' influence on the final material properties is presented. This protocol results in the repeatable preparation of centimeter-sized alumina monoliths presenting a uni-directional macroporosity and structured mesopores. These monoliths should be of particular interest in high flow rate catalytic applications.

Keywords: porous materials; alumina; ice templating; ordered mesoporous alumina

1. Introduction

The porous structure of a solid largely dictates its interaction with liquids and gases along with physical properties such as density, thermal conductivity, and strength. Thus, the fine control of this porous structure is of primary importance for the engineering of industrial catalysts, adsorbents, membranes, and ceramics [1]. While a variety of porous materials can be processed industrially, the attention is particularly focused on alumina-based materials owing to their importance in industrial catalytic processes. Among their numerous advantages one may consider their availability, their Lewis acidic strength, their high mechanical resistance and hydro-thermal stability, and their facile functionalization.

Gamma-alumina is of particular interest due to its important specific surface area that results from the self-stacking of nanosized alumina platelets. However, when bulky molecules with large kinetic diameters are present, such as found in oil refineries, petrochemistry and biomass catalytic conversion, significant diffusion restrictions occur. This motivates both industry and academic research to increase the pore size of alumina. Following the discovery of mesoporous silica-based materials [2–4], Vaudry *et al.* reported the first synthesis of mesoporous alumina materials from aluminium alkoxides using carboxylic acids with a long alkyl chain [5]. Concomitantly, Bagshaw *et al.* obtained alumina with a well-defined mesoporosity using non-ionic polymers [6,7]. These works paved the way for further preparation of alumina-based materials with a controlled mesoporosity following addition of porogens. Several reviews of the development of these materials can be found [8–10].

Pseudoboehmite particles, which are the precursors of gamma-alumina, are generally prepared following a sol-gel process thoroughly investigated by Yoldas in the 80′ s [11,12]. Typical reactants are aluminium alkoxides [$Al(OR)_3$] or salts [$Al(R')_3$], which undergo hydrolysis in the presence of wetness. Those hydrolyzed precursors will polycondensate via oxygen covalent bonding [Al–O–Al], forming a colloidal solution of small oligomers (sol). Further condensation of those oligomers induces the formation of a diphasic system containing both liquid and solid phases (gel). The peptization step that corresponds to the addition of an acid allows dispersion of the colloidal particles. Formation of mesostructured alumina-based materials requires the presence of porogens, which can be classified into three categories: surfactants, non-surfactant organic templates, and inorganic templates. Surfactants, which are amphiphilic molecules, are the most commonly used porogens in sol-gel processes. They are generally dispersed in the presence of small colloids, at a concentration below their critical micellar concentration (cmc). Further progressive evaporation of the solvent concentrates the surfactants until their cmc is reached, driving their organization into liquid crystalline mesophases. This method is known as the evaporation-induced self-assembly (EISA) [13,14]. After thermal treatment, the surfactant is removed, creating the mesoporosity while converting pseudoboehmite particles into gamma-alumina. Owing to their higher mass transfer, such mesoporous materials were successfully applied to the following catalytic reactions: hydrotreatment [15,16], hydrocracking [17], dehydration [18], reforming [19], oxidation [20], and metathesis [21,22].

Up until now, most of material syntheses have focused solely on generating and tuning mesoporosity, largely ignoring the benefits of hierarchical porous networks including macropores that can act as rapid transport channels to the active sites. Simulations show that in the Knudsen diffusion regime, where molecules are able to circulate through mesopores but experience diffusion limitations, an interconnected network of mesopores and macropores could significantly improve the catalyst activity [23]. Multiporous gamma-alumina powders can be obtained by combining surfactants and macropore forming methods such as inverse opals [24], foaming [25], or spinodal decomposition [26]. Those powders present higher diffusivity properties and lower sensibility to deactivation, which is translated in catalysis by higher conversion and selectivities over time [26–29]. However, the macropores formed by these methods are tortuous, thus presenting significant pressure drop in high flow rate applications. One may also note that, for industrial applications, powders must first be shaped into extrudates, granulates, pellets or monoliths in order to facilitate their loading and unloading. Monoliths are particularly advantageous in the case of high flow rate applications as they allow for faster mass and heat transport. An ideal catalytic support would thus be a gamma-alumina monolith presenting interconnected mesopores and straight macropores.

Lately, we reported the preparation of multiporous silica monoliths based on ice-templating: the freezing-induced self-assembly (FISA) process [30]. Ice-templating takes advantage of ice crystal growth to yield micrometer-sized macropores upon sublimation [31]. Under unidirectional solidification conditions, and without any additive, the c-axis of the hexagonal ice crystals is nearly aligned with the temperature gradient, leading to a lamellar morphology. As the solubility limit of almost any compound in ice is extremely low (around 10^{-6} g/L), any species present in the initial suspension will be rejected by the growing crystals. The progressive concentration of surfactants between the ice crystals triggers their self-assembly into organized micellar structures [30]. This technique, which combines ice-templating, surfactant self-assembly, and sol-gel chemistry, should thus be suitable for the preparation of multiporous gamma-alumina monoliths.

However, while the syntheses of mesoporous silica and alumino-silica are nowadays well-described, few studies aimed to better understand alumina-based systems. This is mostly due to the high reactivity of aluminium precursors toward hydrolysis and condensation, favoring the fast precipitation of boehmite platelets [32]. Multiple parameters, sometimes acting synergistically, dictate the degree of ordering, the textural properties, or the acidity of the resulting materials. We thus expect the formation of multiporous alumina monoliths via ice-templating to be sinuous, and conducted a systematic study of the synthesis parameters influence. Our goal is the reproducible preparation of

gamma-alumina monoliths with interconnected ordered mesopores and straight macropores for high flow rate catalytic applications.

2. Results and Discussion

The usual solvent for ice-templating is water. Other solvents, such as tert-butyl alcohol or camphene can be used, but their impact on the surfactant self-assembly needs to be investigated first. The well-known Yoldas process that allows the preparation of colloidal boehmite from aluminium alkoxides has been used here [11,12]. Typically, an aluminium alkoxide was refluxed at 85 °C for 1 h prior to peptization using nitric acid. After ageing at 85 °C, a surfactant was added. The resulting suspension was then ice-templated and freeze-dried. Finally, the monoliths were thermally treated to remove the surfactant and free the mesoporosity. From this initial protocol, 13 parameters—divided into four categories (Table 1)—were identified to potentially impact the final properties of our ice-templated monoliths. Note that these parameters may be interdependent.

Table 1. Parameters having an influence over the material final properties. The parameters studied herein are in bold.

Formulation	Synthesis	Ice-Templating	Thermal Treatment
H_2O/Al ratio	**Temperature**	**Freezing speed**	**Heating rate**
Acid/Al ratio	**Peptization duration**	**H_2O/Al ratio**	**Dwelling temperature**
Acid source	Ageing duration		**Dwelling time**
Surfactant/Al ratio			
Surfactant source			
Alumina source			

This work consisted in the systematic study of those parameters. Aluminium tri sec-butoxide ($Al(O–But)_3$) was used as the aluminium alkoxide, as it was largely used in Yoldas works. P123, a triblock copolymer with general formula $(EO)_{20}(PO)_{70}(EO)_{20}$, was used as the surfactant. Emphasis was given to the influence of parameters on the mesoporosity, without a systematic description of the macroporosity as all the products were centimeter-sized monoliths with a lamellar macroporosity, which is described for one particular multiporous monolith at the end of the paper.

2.1. Determination of Synthesis Parameters

2.1.1. P123/Al Ratio

In the literature, organized mesoporous alumina are usually obtained using P123/Al molar ratio ranging from 0.01 to 0.017 [14,33,34], with exception of the pioneer works of Bagshaw and Pinnavaia where molar ratio up to 1 was used [7]. We thus focused on P123/Al molar ratio in the 0.005–0.016 range. Figure 1 shows that for our synthesis conditions, a P123/Al molar ratio of 0.005 was insufficient to obtain a structured porosity, while molar ratio of 0.01 and above led to comparable mesostructuration results. The unique, large low-angle diffraction peak is characteristic of a worm-like arrangement, meaning that mesopores are uniform but show no long-range order between the pores. This is in accordance with the results reported from water-based systems. We thus decided to use a P123/Al molar ratio of 0.010 for the rest of this study, as using more surfactant than necessary could be detrimental for industrial applications.

2.1.2. Acid Source and Acid/Al Ratio

The nature and quantity of acid are known to have a large impact on the P123 organisation into micelles and further mesophases, as well as on the colloid formation. Yoldas studied the effect of several acids on the peptization step and evidenced two general requirements [11]. First, the acid must be non-complexing (or at least very weakly complexing) with aluminium ions. Second, it must be

sufficiently strong to produce the charge effect in relatively low quantities to avoid the formation of a continuous network through oxalated or oleated bonds. Several inorganic and organic acids, listed in Table 2, were added during the peptization step at constant H^+/Al molar ratio and their impact on the mesostructuration was investigated.

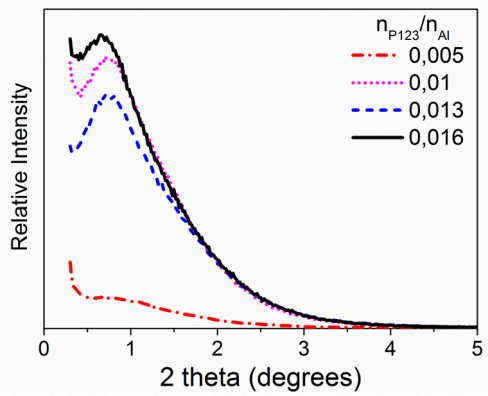

Figure 1. Small angle XRD for P123/Al molar ratios ranging from 0.005 to 0.016.

Table 2. Textural properties and small angle XRD peak position for samples processed using different acids. Samples were thermally treated at 550 °C prior analysis.

Acid	Aspect of Al Sol	H^+/Al Ratio	Peak (nm)	SSA (m^2/g)	V_{porous} (cm^3/g)	d_{porous} (nm)
Sulfuric acid	Yellow opaque	0.10	Could not be ice-templated			
Acetic acid	White opaque	0.10	No peak	222	0.64	10.6
Citric acid	White opaque	0.10	17.7	310	1.13	10.7
Propionic acid	translucent	0.10	13.8	324	0.94	8.4
Chlorhydric acid	translucent	0.10	15.7	328	0.91	8.1
Nitric acid	translucent	0.038	16.7	317	1.11	10.9
Nitric acid	translucent	0.07	11.18	317	0.90	8.4
Nitric acid	translucent	0.10	10.8	327	1.00	8.9
Nitric acid	translucent	0.13	10.6	287	0.72	7.4

It was not possible to process ice-templated monoliths using sulfuric acid due to the resulting high viscosity. This could be due to SO_4^{2-} ions that strongly complex aluminium ions [11]. Acetic acid, even though reported to give clear sols [11,35,36], and citric acid led to a viscous and opaque aspect with visible flocculation. They were ice-templated as-is. All other acid sources gave clear sols and were processed normally. Small angle XRD patterns (Figure S1) show that apart when using acetic acid, a unique and large peak characterizes every processed sample. Using nitric acid, this peak is shifted towards higher 2 theta values, which could characterize smaller ordered mesopores.

The impact of the acid nature on the final textural properties was investigated using nitrogen physisorption (Figure S2). Acetic and citric acids lead to poor pseudoboehmite dispersions, resulting in larger pore size distributions and also to a significantly lower specific surface area in the case of acetic acid. The presence of a well-defined diffraction peak using citric acid might result from a partial organization, but further investigations are necessary to understand its influence on peptization and mesophase organization. Classic type IV isotherms were obtained for samples prepared using propionic, chlorhydric and nitric acids with comparable specific surface areas (SSA, from 325 to 330 m^2/g) and pore volumes (V_{porous} from 0.9 to 1 cm^3/g). However, chlorhydric and propionic acids led to the formation of larger pore sizes compared to nitric acid.

Manet *et al.* studied the impact of several acids on the micellization of P123 by SANS and SAXS. They showed that the overall size of P123 micelles increase following the Hofmeister anions series due

to their salting-in/out properties: NO_3^- < Br^- < Cl^- < SO_4^{2-} < $H_2PO_4^-$ [37]. The salting-out ions Cl^-, SO_4^{2-} and $H_2PO_4^-$ do not show a specific tendency to confine within the micelles. Therefore micelle sizes in their presence are similar. As· NO_3^- is a salting-in ion, its concentration in the outer shell of P123 micelles—composed of hydrophilic EO blocks—should be higher than in the bulk solution [37,38], whereas the concentration of salting-out ions is homogeneous. Ordered mesoporous alumina are thought to form through interactions between charged alumina colloids and the EO blocks of the surfactant [39]. NO_3^- ion enrichment at the micellar interface may bridge the EO blocks and the peptized pseudoboehmite surface. Moreover, NO_3^- ions produce a strong double layer at the pseudoboehmite surface leading to better dispersion [40]. Nitric acid, classically used in the Yoldas process, has therefore been chosen and the impact of nitric acid concentration was further investigated.

Yoldas showed that a clear sol retaining its integrity during hydrolysis and gelation is obtained for acid/Al molar ratio comprised between 0.03 and 0.1 [11]. The impact of nitric acid content was evaluated for ratios ranging from 0.038 to 0.13. The characteristic large diffraction peak (Figure S3) representative of mesoscopic ordering is observed for all studied HNO_3/Al ratios. The peak position is shifted towards smaller angles for the 0.038 ratio, but is similar for ratios ranging from 0.07 to 0.13. Broader pore size distributions (Figure 2 and Figure S4) are observed for the two extreme HNO_3/Al molar ratios: 0.038 and 0.13. The shoulder centered around 4 nm on the pore size distribution is typical of partial aggregation of boehmite particles [41]. The narrowest pore size distribution is observed for a HNO_3/Al molar ratio of 0.07, which corresponds to optimal interparticle repulsions in boehmite sols [12]. Lower, however, sufficient repulsions allow for closer boehmite particles packing, and thus better replication of the P123 micelles. This concentration was thus kept constant while other parameters were varied.

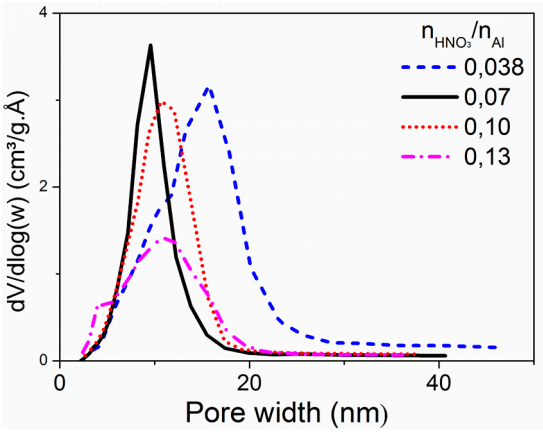

Figure 2. Pore size distributions for samples synthesized using different HNO_3/Al molar ratios.

2.1.3. Impact of Peptization Duration and Temperature

The peptization step is critical for a proper dispersion of the pseudoboehmite. Hence, insufficient peptization duration or temperature may affect the overall mesostructuration of the material. Amorphous aluminium hydroxide is formed at room temperature, whereas temperatures above 85 °C are needed to form pseudoboehmite [11,42]. The boehmite crystallite size increases linearly with time until peptization, which inhibits further growth. An ageing step of 1 h was maintained prior to peptization to ensure complete hydrolysis of the alkoxide while keeping boehmite crystallite size small enough to fit into inter-micellar voids. Martens *et al.* [42] proposed that the peptization mechanism is linked to the particle growth as platelets before peptization and their further stacking. Faster peptization leads to increased surface area and larger interparticle porosity. Moreover, the *n*-butanol formed during the alkoxide hydrolysis may block pores and impede the needed acid adsorption.

We studied the impact of peptization duration on the mesophase formation at two temperatures: 85 and 100 °C. Figure 3 shows that the organization of the mesostructure is linked to the peptization

conditions: at 85 °C, a distinct diffraction peak is observed after long peptization times, whereas this peak is already present after 2 h of peptization at 100 °C. The presence of mesoscopic organization can be linked to close packing of the boehmite particles around the P123 micellar mesophase, which is favored at high particle dispersion. This trend is confirmed by N_2 isotherms (Figure 4 and Figure S5). At 85 °C, the population of 4–5 nm pores linked to pseudoboehmite particles' aggregation tends to reduce with peptization time. At 100 °C, pores corresponding to P123 micelles' replication are largely predominant, meaning that peptization was already complete after 2 h. The pore size distribution shifts towards smaller diameters with increasing peptization time. TEM analysis of the pseudo-boehmite hydrosol respectively after 20 h at 85 °C and 6 h at 100 °C, show that both synthesis conditions lead to pseudoboehmite crystallization (Figure S6). The protocol was then adjusted using 100 °C as the synthesis temperature and peptization duration of 6 h.

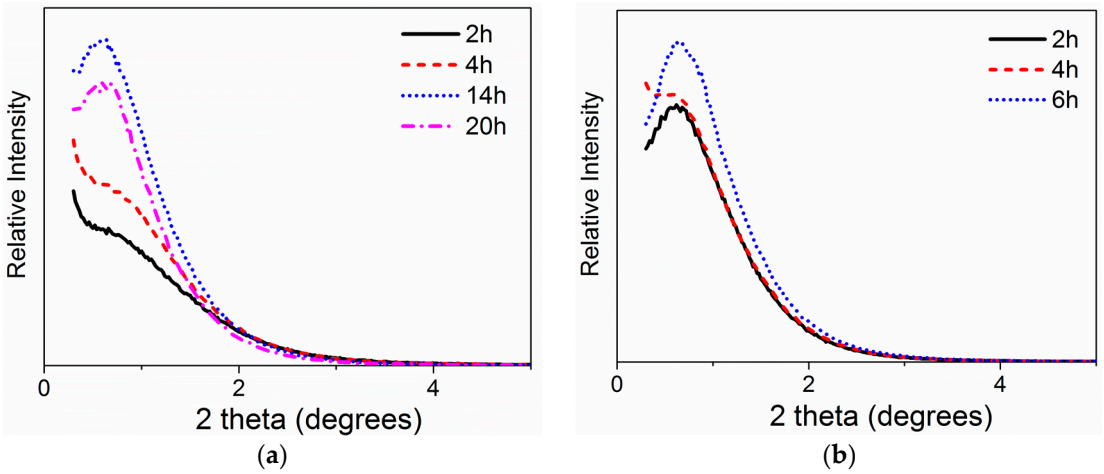

Figure 3. Impact of peptization duration on small angle XRD at (**a**) 85 °C and (**b**) 100 °C.

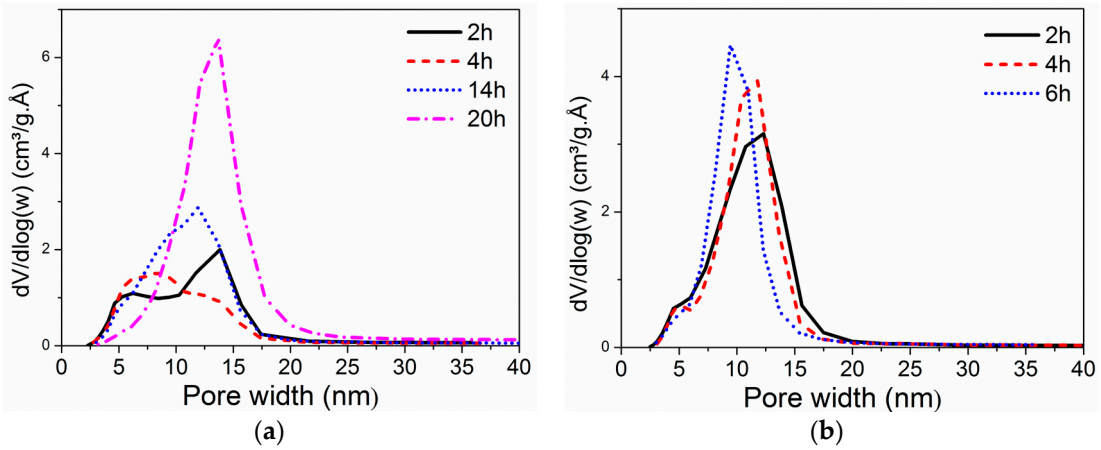

Figure 4. Pore size distribution from N_2 isotherms, impact of peptization at (**a**) 85 °C and (**b**) 100 °C.

2.2. Process Parameters

The first part concluded that the quality of the mesostructuration in these ice-templated meso-macro monoliths seems to be overall linked to two main factors: the size and dispersion of the pseudoboehmite particles, and their close stacking inside the aqueous phase of the lyotropic liquid crystal mesophase. Although all these samples were processed by ice-templating to form monoliths, the impact of the synthesis parameters was also investigated for powders processed by EISA. Comparative small angle XRD and N_2 isotherms are shown in Figures S7 and S8. Similar impacts

on the structural and textural properties can be observed, meaning that our results can be applied to EISA studies and *vice-versa*.

In this second part, we will describe the impact of two process parameters: the water content and the cooling speed.

2.2.1. Water Content

During the ice-templating process, water is solidified into lamellar ice crystals. Thus, the water content defines the macroporosity in the final material. While a water/Al molar ratio of 100 is usual for the Yoldas process, such high water content does not lead to the formation of stable monoliths. From a H_2O/Al molar ratio of 50, allowing the formation of stable monoliths, the water content was progressively decreased until the viscosity of the sol prevented processing, *i.e.*, down to a H_2O/Al molar ratio of 15. For such low water contents, samples were heterogeneous after ice-templating. Moreover, Figure 5 shows that the mesostructuration disappears at this H_2O/Al ratio and a significant contribution of non-dispersed pseudoboehmite particles is present in the pore size distribution (Figure S9). Hereafter, a H_2O/Al molar ratio of 25 was used.

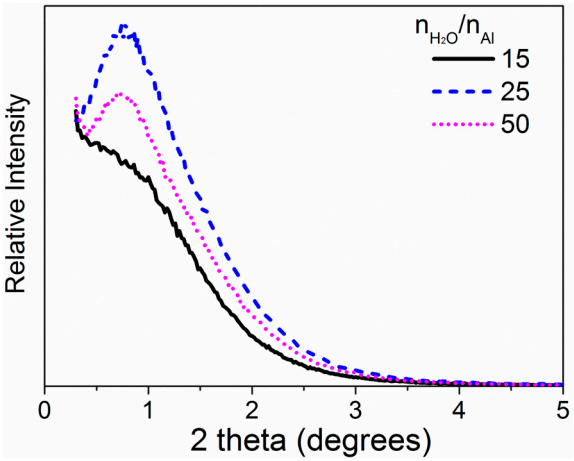

Figure 5. Impact of water content on small angle XRD.

2.2.2. Cooling Speed

The cooling speed corresponds to the rate at which the copper plate at the bottom of the slurry is cooled, leading to ice crystals' nucleation and growth. The cooling speed directly impacts the ice crystals' growth velocity. During growth, all compounds are progressively rejected and concentrated between the ice crystals. This concentration mechanism previously allowed P123 self-organization and further mesostructuration of a silica monolith [30]. The ice growth velocity controls the kinetics of P123 self-organization and the boehmite crystals' close packing [41] in the aqueous part of the lyotropic liquid crystal mesophase. Two cooling rates were tested: -2 °C/min and -10 °C/min. Figure 6 shows that if the freezing front is moving too fast (cooling rate of -10 °C/min), no mesostructuration is obtained. The corresponding isotherms show a larger pore size distribution, probably linked to lower stacking control of the particles. Nevertheless, the ice growth velocity influences neither the pore volume (0.93 $cm^2 \cdot g^{-1}$), nor the surface area of the material (265 $m^2 \cdot g^{-1}$). Thus, the mesoporosity was fully retained. Following those observations, a cooling rate of -2°C/min was used to process a batch of samples in order to study the influence of the thermal treatment over the final textural and structural properties.

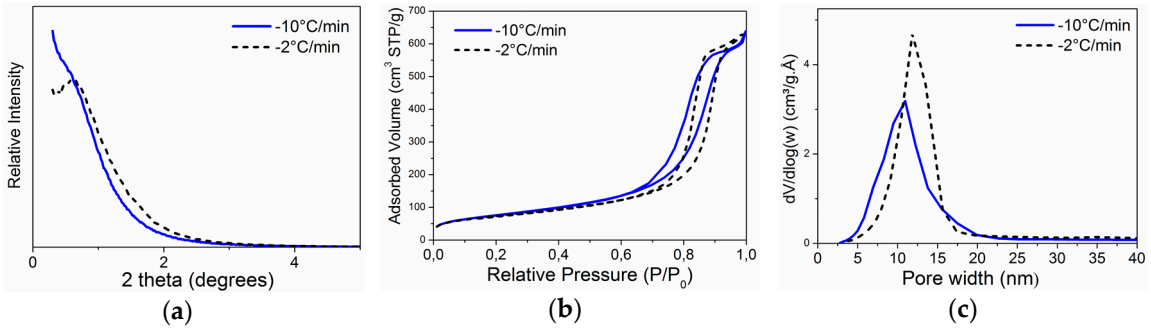

Figure 6. Impact of cooling speed on (**a**) XRD; (**b**) N_2 isotherm and (**c**) pore size distribution.

2.3. Thermal Stability

A thermal treatment at 550 °C is sufficient to remove the P123 surfactant, as determined by TGA-DSC (Figure S10) and leads to gamma-alumina (γ-Al_2O_3). Catalytic tests, however, are often performed at higher temperatures and it is thus important to study the impact of temperature on the alumina phase and the mesoporosity. The small angle diffraction peak corresponding to mesoscopic order is clearly visible up to 850 °C (Figure 7a), then transforming into a shoulder of the incident beam and disappearing above 1000 °C. The high angle XRD analysis (Figure 7b) shows that at 550 °C, the sample is composed of low crystallized γ-Al_2O_3 particles. The loss of mesoscopic ordering at 900 °C is related to the appearance of a theta-alumina (θ-Al_2O_3) phase. With increasing temperature, the proportion of θ-Al_2O_3 increases at the expense of the γ-Al_2O_3 phase. The pore volume also remains constant up to 900 °C (Table 3, Figure S11), then decreases rapidly with the calcination temperature. This is linked to the progressive transformation of γ-Al_2O_3 into θ-Al_2O_3 and the resulting global particle size increase. Nevertheless, mesoporosity is maintained up to 1050 °C, with a still consequent specific surface area. For catalytic applications, γ-Al_2O_3 is usually targeted, limiting the final thermal treatment temperature to 850 °C. Under these conditions, specific surface areas higher than 250 m^2/g are observed.

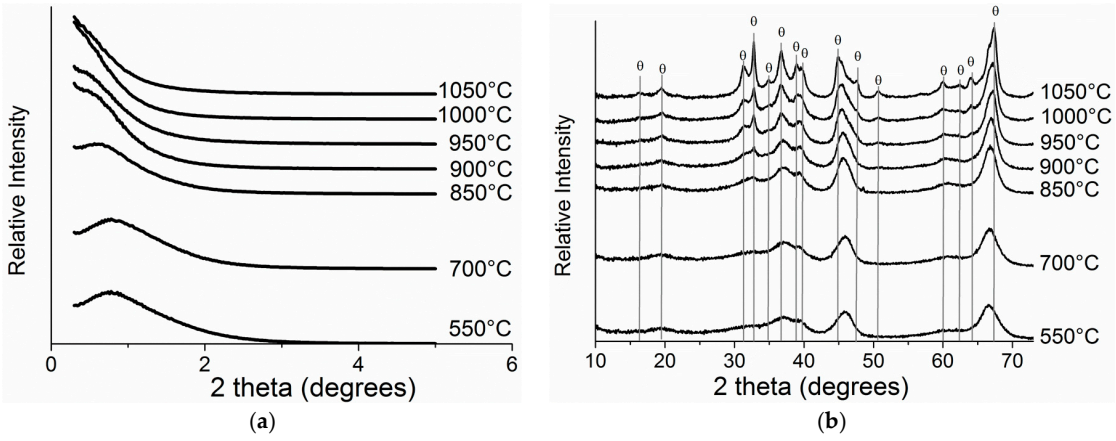

Figure 7. Impact of the thermal treatment by (**a**) small angle XRD; (**b**) wide angle XRD.

Table 3. Textural properties as a function of calcination temperature.

Calcination Temperature (°C)	SSA (m^2/g)	V_{porous} (cm^3/g)	d_{pores} (nm)
550	317	0.90	8.4
850	260	0.95	11.2
900	236	0.91	11.1
950	188	0.71	11.6
1000	210	0.82	11.7
1050	127	0.54	14.4

2.4. Macroporosity

Emphasis has been so far given to the impact of formulation and process parameters on mesoporosity. However, all samples were systematically processed as monoliths (Figure 8a), comprising an ice-templated macroporosity. Figure 8b–f shows SEM images representative of the lamellar macroporosity. Sublimation of the ice crystals leads to the formation of 50 µm × 25 µm macropores in the final material (Figure 8b,c). The walls in-between the macropores are a few µm in thickness and porous throughout (Figure 8f). Parallel to the freezing direction (Figure 8d,e), dendrites can be seen, adding rugosity to the macroporous channels. High magnification of the inorganic walls surface (Figure 8e) shows that the in-wall mesoporosity is accessible from the macropores. This was further confirmed by mercury porosimetry (Figure S12), which reveals several lengths of interconnected porosity. The 0.01 µm pore size contribution corresponds to the mesoporosity described up to now, also indicating that these pores are accessible from the macropores. The contribution of the ice-templated macropores corresponds to the pore diameters above 1 µm.

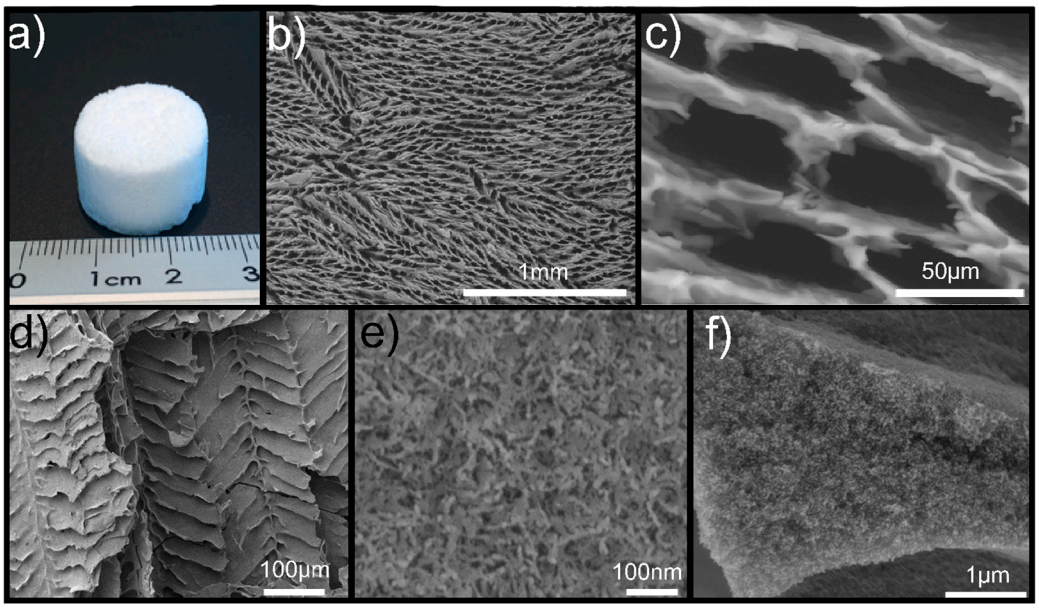

Figure 8. Ice templated γ-alumina monolith with hierarchical porosity (**a**) Photography; (**b**,**c**,**f**) SEM micrographs showing the ice-templated macroporosity perpendicular to the freezing direction; (**d**,**e**) parallel to the freezing direction.

3. Experimental Section

3.1. Synthesis

Boehmite nanoparticles were synthesized following the procedure reported by Yoldas [11,12]. If not stated otherwise, aluminium tri sec-butoxide ($Al(O–But)_3$, 97%, Sigma-Aldrich, St. Louis,

MO, USA) was refluxed at 85 °C for 1 h. Then, nitric acid (67%, Sigma-Aldrich) was added for peptization, leading to a transparent sol. The suspension was aged by refluxing for 16 h at 85 °C, then the triblock copolymer P123:$(EO)_{20}(PO)_{70}(EO)_{20}$ (Poly(ethylene glycol)-*block*-poly(propylene glycol)-*block*-poly(ethylene glycol); average Mn 5800 g/mol, Sigma-Aldrich) was added. The suspension was refluxed for an additional hour at the same temperature to insure complete dissolution of the P123. The typical molar composition of the hydrosol was 1 Al:50 H_2O:0.01 P123:0.07 HNO_3. In this study, P123 was varied from 0.005 to 0.016, H_2O was varied from 10 to 50, and the acid was varied from 0.07 to 0.13. The impact of several acids was evaluated. In this case, the H^+/Al ratio was kept constant.

3.2. Materials Processing

The suspension was typically poured into 1 cm diameter PTFE molds, placed on a copper plate. This copper plate was cooled at constant cooling rate of −2 °C/min until complete freezing of the suspension. The cooling rate was controlled by a thermocouple located inside the copper plate and connected to a Huber CC 905 cryothermostat [30]. Alternatively, the PTFE molds were placed on the top of copper rods, then sunken in a liquid nitrogen-filled Dewar. In this configuration, the cooling rate is driven by the thermal conductivity of the rod. Herein, copper rods allow reaching a cooling rate of about −10 °C/min. After complete freezing, the samples were demolded, then placed for 48 h in a Labconco FreeZone 2.5 freeze-dryer to sublime the ice crystals (−80 °C; 0.120 mbar).

Mesoporous powders were prepared by evaporation of the suspension under reduced pressure in a rotavapor at 40 °C until a dry powder was obtained.

The final material was typically thermally treated at 550 °C for 2 h with a heating rate of 5 °C/min. The impact of the thermal treatment was studied between 550 and 1050 °C. Heating rates were varied from 0.2 to 5 °C per minute and dwelling times at final temperature from 1 to 5 h.

3.3. Material Characterization

Small-angle powder X-ray diffraction patterns were recorded with a 0.05° step size (step time = 1 s) on a Siemens D5000 X-ray diffractometer equipped with a CuKα_1 monochromatic radiation source (40 kV, 35 mA) and a 0.1 mm reception slit. Nitrogen physisorption was performed on a Micromeritics Tristar II instrument, after treatment of the samples under primary vacuum (20 mTorr) at 280 °C overnight. Surface areas were calculated using the Brunauer-Emmett-Teller (BET) method over the range P/P0 = 0.07–0.30, where a linear relationship was maintained. Mesopore size distributions were calculated using the Barrett–Joyner–Halenda (BJH) model applied to the desorption branch of the isotherm. Mesopore volumes were evaluated on the volume adsorbed at P/P0 = 0.99. Mercury intrusion porosimetry was performed on a Micromeritics AutoPore IV 9500. TGA-DSC measurements were performed under air with a heating rate of 5 °C per minute from room temperature to 1100 °C using a SETARAM Model TGA92 S/N 31/8178. Scanning electron micrographs were acquired on a scanning electron microscope FEI Nova NanoSEM 230. Prior analysis, a thin coating of platinum was deposited onto the samples. High-resolution transmission electron microscopy was carried out by using a FEI Tecnai G2 20 operating at 200 kV. Samples were prepared by depositing a drop of solution containing the sample in ethanol on a holey-carbon film copper grid.

4. Conclusions

Macro-mesoporous alumina monoliths were synthesized following a combination of sol-gel chemistry, P123 self-assembly and ice-templating. The use of this latter process required the development of a pure water-based synthesis of mesoporous alumina. Such a synthesis is not usual for the preparation of mesoporous alumina powders, as most of the protocols described in the literature use alcohols. The systematic study presented here concluded that the quality of the mesoporosity is directly linked to the synthesis, which controls the size of the precipitated particles and the quality of the boehmite dispersion. The best mesophase organization was found for the parameters leading

to small pseudoboehmite particles, peptized under conditions optimizing interparticle repulsions. We also proposed a mechanism for the improved results obtained with nitric acid, based on the bridging effect of NO_3^- between the EO blocks of the triblock copolymer and the pseudoboehmite particles. Such multiporous alumina monoliths may provide new opportunities as supports in high flow rate applications. We are currently investigating their use as catalytic supports for the continuous conversion of bulky molecules.

Supplementary Materials: Supplementary materials can be accessed at www.mdpi.com/2304-6740/4/1/6/s1.

Acknowledgments: Saint-Gobain is acknowledged for financial support of this work. Ahmed Addad is acknowledged for help with the TEM imaging. The TEM facility in Lille (France) is supported by the Conseil Regional du Nord-Pas de Calais, and the European Regional Development Fund (ERDF).

Author Contributions: Jérémy Dhainaut, Sylvain Deville, Idris Amirouche and Michaela Klotz designed the research. Jérémy Dhainaut performed the experimental work. All authors analyzed and discussed the results. Jérémy Dhainaut, Sylvain Deville and Michaela Klotz wrote the paper.

Conflicts of Interest: The authors declare no conflict of interest.

References

1. Rouquerol, J.; Avnir, D.; Fairbridge, C.W.; Everett, D.H.; Haynes, J.H.; Pernicone, N.; Ramsay, J.D.F.; Sing, K.S.W.; Unger, K.K. Recommendations for the characterization of porous solids. *Pure Appl. Chem.* **1994**, *66*, 1739–1758. [CrossRef]
2. Kresge, C.T.; Leonowicz, M.E.; Roth, W.J.; Vartuli, J.C.; Beck, J.S. Ordered mesoporous molecular sieves synthesized by a liquid-crystal template mechanism. *Nature* **1992**, *359*, 710–712. [CrossRef]
3. Beck, J.S.; Vartuli, J.C.; Roth, W.J.; Leonowicz, M.E.; Kresge, C.T.; Schmitt, K.D.; Chu, C.T.-W.; Olson, D.H.; Sheppard, E.W.; McCullen, S.B.; *et al*. A new family of mesoporous molecular sieves prepared with liquid crystal templates. *J. Am. Chem. Soc.* **1992**, *114*, 10834–10843. [CrossRef]
4. Chiola, V.; Ritsko, J.E.; Clarence, D. Process for Producing Low-Bulk Density Silica. U.S. Patent 3,556,725, 19 January 1971.
5. Vaudry, F.; Khodabandeh, S.; Davis, M.E. Synthesis of pure alumina mesoporous materials. *Chem. Mater.* **1996**, *8*, 1451–1464. [CrossRef]
6. Bagshaw, S.A.; Prouzet, E.; Pinnavaia, T.J. Templating of mesoporous molecular sieves by nonionic polyethylene oxide surfactants. *Science* **1995**, *269*, 1242–1244. [CrossRef] [PubMed]
7. Bagshaw, S.A.; Pinnavaia, T.J. Mesoporous alumina molecular sieves. *Angew. Chem. Int. Ed. Engl.* **1996**, *35*, 1102–1105. [CrossRef]
8. Soler-Illia, G.J.D.A.; Sanchez, C.; Lebeau, B.; Patarin, J. Chemical strategies to design textured materials: From microporous and mesoporous oxides to nanonetworks and hierarchical structures. *Chem. Rev.* **2002**, *102*, 4093–4138. [CrossRef] [PubMed]
9. Sanchez, C.; Boissière, C.; Grosso, D.; Laberty, C.; Nicole, L. Design, synthesis, and properties of inorganic and hybrid thin films having periodically organized nanoporosity. *Chem. Mater.* **2008**, *20*, 682–737. [CrossRef]
10. Márquez-Alvarez, C.; Žilková, N.; Pérez-Pariente, J.; Čejka, J. Synthesis, characterization and catalytic applications of organized mesoporous aluminas. *Catal. Rev.* **2008**, *50*, 222–286. [CrossRef]
11. Yoldas, B. Alumina sol preparation from alkoxides. *Ceram. Bull.* **1975**, *54*, 289–290.
12. Yoldas, B.E. Alumina gels that form porous transparent Al_2O_3. *J. Mater. Sci.* **1975**, *10*, 1856–1860. [CrossRef]
13. Brinker, C.J.; Lu, Y.; Sellinger, A.; Fan, H. Evaporation-induced self-assembly: Nanostructures made easy. *Adv. Mater.* **1999**, *11*, 579–585. [CrossRef]
14. Yuan, Q.; Yin, A.-X.; Luo, C.; Sun, L.-D.; Zhang, Y.-W.; Duan, W.-T.; Liu, H.-C.; Yan, C.-H. Facile synthesis for ordered mesoporous γ-aluminas with high thermal stability. *J. Am. Chem. Soc.* **2008**, *130*, 3465–3472. [CrossRef] [PubMed]
15. Valange, S.; Barrault, J.; Derouault, A.; Gabelica, Z. Binary Cu–Al mesophases precursors to uniformly sized copper particles highly dispersed on mesoporous alumina. *Microporous Mesoporous Mater.* **2001**, *44–45*, 211–220. [CrossRef]
16. Liu, Q.; Wang, A.; Wang, X.; Gao, P.; Wang, X.; Zhang, T. Synthesis, characterization and catalytic applications of mesoporous γ-alumina from boehmite sol. *Microporous Mesoporous Mater.* **2008**, *111*, 323–333. [CrossRef]

17. Looi, P.Y.; Mohamed, A.R.; Tye, C.T. Hydrocracking of residual oil using molybdenum supported over mesoporous alumina as a catalyst. *Chem. Eng. J.* **2012**, *181–182*, 717–724. [CrossRef]
18. Khaleel, A. Methanol dehydration to dimethyl ether over highly porous xerogel alumina catalyst: Flow rate effect. *Fuel Process. Technol.* **2010**, *91*, 1505–1509. [CrossRef]
19. Newnham, J.; Mantri, K.; Amin, M.H.; Tardio, J.; Bhargava, S.K. Highly stable and active Ni-mesoporous alumina catalysts for dry reforming of methane. *Int. J. Hydrog. Energy* **2012**, *37*, 1454–1464. [CrossRef]
20. Nie, L.; Meng, A.; Yu, J.; Jaroniec, M. Hierarchically macro-mesoporous Pt/γ-Al_2O_3 composite microspheres for efficient formaldehyde oxidation at room temperature. *Sci. Rep.* **2013**, *3*. [CrossRef] [PubMed]
21. Oikawa, T.; Ookoshi, T.; Tanaka, T.; Yamamoto, T.; Onaka, M. A new heterogeneous olefin metathesis catalyst composed of rhenium oxide and mesoporous alumina. *Microporous Mesoporous Mater.* **2004**, *74*, 93–103. [CrossRef]
22. Hamtil, R.; Žilková, N.; Balcar, H.; Čejka, J. Rhenium oxide supported on organized mesoporous alumina—A highly active and versatile catalyst for alkene, diene, and cycloalkene metathesis. *Appl. Catal. A Gen.* **2006**, *302*, 193–200. [CrossRef]
23. Gheorghiu, S.; Coppens, M.-O. Optimal bimodal pore networks for heterogeneous catalysis. *AIChE J.* **2004**, *50*, 812–820. [CrossRef]
24. Dacquin, J.-P.; Dhainaut, J.; Duprez, D.; Royer, S.; Lee, A.F.; Wilson, K. An efficient route to highly organized, tunable macroporous-mesoporous alumina. *J. Am. Chem. Soc.* **2009**, *131*, 12896–12897. [CrossRef] [PubMed]
25. Li, L.-L.; Duan, W.-T.; Yuan, Q.; Li, Z.-X.; Duan, H.-H.; Yan, C.-H. Hierarchical γ-Al_2O_3 monoliths with highly ordered 2D hexagonal mesopores in macroporous walls. *Chem. Commun.* **2009**, 6174–6176. [CrossRef] [PubMed]
26. Yabuki, M.; Takahashi, R.; Sato, S.; Sodesawa, T.; Ogura, K. Silica-alumina catalysts prepared in sol-gel process of TEOS with organic additives. *Phys. Chem. Chem. Phys.* **2002**, *4*, 4830–4837. [CrossRef]
27. Han, D.; Li, X.; Zhang, L.; Wang, Y.; Yan, Z.; Liu, S. Hierarchically ordered meso/macroporous γ-alumina for enhanced hydrodesulfurization performance. *Microporous Mesoporous Mater.* **2012**, *158*, 1–6. [CrossRef]
28. Vinogradov, V.V.; Vinogradov, A.V.; Kraev, A.S.; Agafonov, A.V.; Kessler, V.G. Sol-gel synthesis, characterization and catalytic activity of γ-alumina with bimodal mesopore distribution. *J. Sol-Gel Sci. Technol.* **2013**, *68*, 155–161. [CrossRef]
29. Zhang, Y.; Zhao, C.Y.; Liang, H.; Liu, Y. Macroporous monolithic Pt/γ-Al_2O_3 and K–Pt/γ-Al_2O_3 catalysts used for preferential oxidation of CO. *Catal. Lett.* **2008**, *127*, 339–347. [CrossRef]
30. Dhainaut, J.; Piana, G.; Deville, S.; Guizard, C.; Klotz, M. Freezing-induced ordering of block-copolymer micelles. *Chem. Commun.* **2014**, *50*, 12572–12574. [CrossRef] [PubMed]
31. Deville, S. Ice-templating, freeze casting: Beyond materials processing. *J. Mater. Res.* **2013**, *28*, 2202–2219. [CrossRef]
32. Schüth, F. Non-siliceous mesostructured and mesoporous materials. *Chem. Mater.* **2001**, *13*, 3184–3195. [CrossRef]
33. Zhang, Z.; Hicks, R.W.; Pauly, T.R.; Pinnavaia, T.J. Mesostructured forms of γ-Al_2O_3. *J. Am. Chem. Soc.* **2002**, *124*, 1592–1593. [CrossRef] [PubMed]
34. Hartmann, S.; Sachse, A.; Galarneau, A. Challenges and strategies in the synthesis of mesoporous alumina powders and hierarchical alumina monoliths. *Materials* **2012**, *5*, 336–349. [CrossRef]
35. Zakharchenya, R.I. Influence of peptization on the properties of alumina produced from boehmite sols. *J. Sol-Gel Sci. Technol.* **1996**, *6*, 179–186. [CrossRef]
36. Park, M.C.; Lee, S.R.; Kim, H.; Park, I.; Choy, J.H. Tailoring porosity of colloidal boehmite sol by controlling crystallite size. *Bull. Korean Chem. Soc.* **2012**, *33*, 1962–1966. [CrossRef]
37. Manet, S.; Lecchi, A.; Impéror-Clerc, M.; Zholobenko, V.; Durand, D.; Oliveira, C.L.P.; Pedersen, J.S.; Grillo, I.; Meneau, F.; Rochas, C. Structure of micelles of a nonionic block copolymer determined by SANS and SAXS. *J. Phys. Chem. B* **2011**, *115*, 11318–11329. [CrossRef] [PubMed]
38. Manet, S.; Schmitt, J.; Impéror-Clerc, M.; Zholobenko, V.; Durand, D.; Oliveira, C.L.P.; Pedersen, J.S.; Gervais, C.; Baccile, N.; Babonneau, F.; *et al*. Kinetics of the formation of 2D-hexagonal silica nanostructured materials by nonionic block copolymer templating in solution. *J. Phys. Chem. B* **2011**, *115*, 11330–11344. [CrossRef] [PubMed]
39. Fulvio, P.F.; Brosey, R.I.; Jaroniec, M. Synthesis of mesoporous alumina from boehmite in the presence of triblock copolymer. *ACS Appl. Mater. Interfaces* **2010**, *2*, 588–593. [CrossRef] [PubMed]

40. Zamorategui, A.; Martinez, J.M.; Tanaka, S. Maximum solid loading dispersion of pseudoboehmite. *J. Aust. Ceram. Soc. Vol.* **2015**, *51*, 40–46.
41. Klotz, M.; Amirouche, I.; Guizard, C.; Viazzi, C.; Deville, S. Ice templating—An alternative technology to produce micromonoliths. *Adv. Eng. Mater.* **2012**, *14*, 1123–1127. [CrossRef]
42. Martens, W.N.; Kloprogge, J.T.; Frost, R.L.; Bartlett, J.R. A crystallite packing model for pseudoboehmite formed during the hydrolysis of trisecbutoxyaluminium to explain the peptizability. *J. Colloid Interface Sci.* **2002**, *247*, 132–137. [CrossRef] [PubMed]